XX IMEKO World Congress
Metrology for Green Growth
September 9–14, 2012, Busan, Republic of Korea

UNCERTAINTY OF COMPONENTS OF VOLUMETRIC ERRORS

[1]A.R. Valdés, [2]Piratelli-Filho, A./Presenter and [3]D.P. Vieira Sato

[1]Universidade Federal de Uberlândia. Faculdade de Engenharia Mecânica. Uberlândia. MG. Brasil
[2]Universidade de Brasília. Faculdade de Tecnologia. Dpto Engenharia Mecânica. 70910-900. Brasília. DF. Brasil
[3]UniFEI. Av. Humberto de A. C. Branco, 3972 - São Bernardo do Campo - SP- 09850-901.

Abstract: The aim of the present work is to calculate the uncertainty associated with volumetric error components in a Moving Bridge type Coordinate Measuring Machine (CMM). Two methodologies are presented for this purpose. The first consisted in equationing the components of the volumetric error using homogeneous transformations techniques; measurement of the geometric errors and Abbé offsets; mathematical models regarding each geometric error and Abbé offset were written and the law of uncertainty propagation was applied. The second methodology present simplified models to estimate the measurement uncertainty associated with volumetric error component, identifying the variables that influence the determination of geometry deviations, development of a mathematical model for the volumetric error components, development of a routine to evaluate uncertainty. It was concluded that the simplified models are adequate and easy to be applied. As conclusions, the components of volumetric error of X, Y and Z axes present uncertainty values close to 2,7, 4,0 and 2,0 μm, respectively.

Keywords: uncertainty; geometric error; Abbé offset.

1. INTRODUCTION

According to its behavior, the measurement error can be classified as systematic or random. Systematic effects can be corrected without great difficulties; nevertheless, after the correction, a doubt will still remain about how well corrected the value obtained in a measurement is. By adding this doubt to those of systematic and random effects, the conventionally so called measurement uncertainty [1] can be obtained.

At the present time, it is not enough to express the numerical value of the measured errors, arising thus, the need to indicate quantitatively the quality of the result of a measurement. In other words, adding to the result of the measurement a statement about the reliability associated to it, that is, the measurement uncertainty.

2. MEASUREMENT UNCERTAINTY IN CMMs

The evaluation of measuring instruments, such as CMM through measurement uncertainty, is a rather difficult task due to the large number of factors that can contribute to the uncertainty, as well as the machine versatility, which allows measuring several metrological features of a workpiece [2].

The performance of CMM has been limited by several factors, which act together, combining complex ways throughout the working volume of the machine, generating the called volumetric error. The largest contribution to the volumetric error is constituted by geometric errors [3]. These errors have their origin in the geometric deviations of the different components of the Measuring Machine.

In order to study geometric errors, the CMM moving elements are assumed as rigid bodies. The position of a rigid body in space can be defined by six degrees of freedom. Since each degree of freedom can be associated to an error, six geometric errors are associated to each preferential axis of the CMM, specifically, one position error, two straightness errors and three rotation errors (pitch, yaw and roll), summing up a total number of 18 geometric errors. Three more errors must be added due to the impossibility of arranging three perfectly orthogonal axes, namely orthogonal errors, which depend on the relation between components. Therefore, a full amount of 21 errors can be determined from three Cartesian axes CMMs.

It is known that inspections using CMMs are carried out from coordinate points (*Xi*, *Yi* and *Zi*) on a given surface. The coordinates of the points, which are measured by means of an optical-electronic system, are used by the CMM software to identify the geometric features of the workpiece. The real coordinates of the points in the CMM work volume can be determined if the measured coordinates and their respective errors are known, Eq. (1).

$$\begin{aligned} X_{Real} &= X_{Machine} - Ex \\ Y_{Real} &= Y_{Machine} - Ey \\ Z_{Real} &= Z_{Machine} - Ez \end{aligned} \qquad (1)$$

where: $X_{Machine}$, $Y_{Machine}$ and $Z_{Machine}$ are the coordinates of the measured points; X_{Real}, Y_{Real} e Z_{Real} are the ideal or true coordinates and E_x, E_y and E_z are the error components associated to each coordinate.

The uncertainty associated to the real coordinates (X_{Real}, Y_{Real} and Z_{Real}) can be assumed as being equal to zero and the uncertainty associated to coordinates *X*, *Y* and *Z* of the

measured points can be considered equal to the uncertainty obtained for the components of the volumetric error, *Ex*, *Ey* and *Ez*, Eq. (2).

$$\begin{aligned} u(X_{Machine}) &= u(Ex) \\ u(Y_{Machine}) &= u(Ey) \\ u(Z_{Machine}) &= u(Ez) \end{aligned} \tag{2}$$

Therefore, the uncertainty of three-dimensional measurement can be determined from the uncertainties associated to the spatial points that define the sought dimensional feature. Such uncertainty is referred to as three-dimensional or volumetric and is related to a region in space whose shape and size are defined by the combination of the various existing uncertainty sources.

This work presents a methodology to estimate the measurement uncertainty associated to the components of the volumetric error of a moving bridge CMM, aiming, in the future, at the determination of the measurement uncertainty associated to the measurements performed with these machines. All experimental runs for the acquisition of error data were conducted on a Moving Bridge CMM (Fig. 1).

Figure 1. Moving Bridge type CMM.

2.1. First model

The error synthesization model used to estimate uncertainty measurement associated volumetric components errors was developed by [4]. This model was obtained by means of homogeneous transformations, each component of the volumetric error can be described as the sum of different parts that are related to the geometric errors of the machine and to the corresponding Abbè offsets, Eq. (3)-(5).

$$\begin{aligned} Ex = {} & Pos(x) + Ry(x) + Rz(x) + [Ort(xy) + Yaw(x)] \cdot Y_{34} + \\ & + [Ort(xz) + Pitch(x) + Yaw(z) + Roll(y)](-Z - Z_{45}) + \\ & + Roll(y) \cdot Z_{12} \end{aligned} \tag{3}$$

$$\begin{aligned} Ey = {} & Pos(y) + Ry(x) + Ry(z) + \\ & + [Ort(xy) + Yaw(y)] \cdot (X_{23} + X) - Pitch(y) \cdot Z_{12} + \\ & - [Ort(yz) + Roll(x) + Pitch(y) + Pitch(z)](-Z - Z_{45}) \end{aligned} \tag{4}$$

$$\begin{aligned} Ez = {} & Pos(z) + Rx(z) + Ry(z) - \\ & - Roll(y) \cdot (X_{23} + X) - [Roll(x) + Pitch(y)] \cdot Y_{34} \end{aligned} \tag{5}$$

To determinate uncertainty associated to the geometric errors, in the equations (3) - (5) the law of propagation of uncertainty were applied, and equations (6) - (8) obtained.

$$\begin{aligned} u^2 Ex = {} & \left(\frac{\partial Ex}{\partial Pos(x)}\right)^2 u^2_{Pos(x)} + \left(\frac{\partial Ex}{\partial Ry(x)}\right)^2 u^2_{Ry(x)} + \\ & + \left(\frac{\partial Ex}{\partial Rz(x)}\right)^2 u^2_{Rz(x)} + \left(\frac{\partial Ex}{\partial Ort(xy)}\right)^2 u^2_{Ort(xy)} \cdot \left(\frac{\partial Ex}{\partial Y_{34}}\right)^2 u^2_{Y_{34}} + \\ & + \left(\frac{\partial Ex}{\partial Yaw(y)}\right)^2 u^2_{Yaw(y)} \cdot \left(\frac{\partial Ex}{\partial Y_{34}}\right)^2 u^2_{Y_{34}} + \\ & + \left(\frac{\partial Ex}{\partial Ort(xz)}\right)^2 u^2_{Ort(xz)} \cdot \left(\frac{\partial Ex}{\partial(-Z - Z_{45})}\right)^2 u^2_{(-Z-Z_{45})} + \\ & + \left(\frac{\partial Ex}{\partial Pitch(x)}\right)^2 u^2_{Pitch(x)} \cdot \left(\frac{\partial Ex}{\partial(-Z - Z_{45})}\right)^2 u^2_{(-Z-Z_{45})} + \\ & + \left(\frac{\partial Ex}{\partial Yaw(z)}\right)^2 u^2_{Yaw(z)} \cdot \left(\frac{\partial Ex}{\partial(-Z - Z_{45})}\right)^2 u^2_{(-Z-Z_{45})} + \\ & + \left(\frac{\partial Ex}{\partial Ort(xz)}\right)^2 u^2_{Ort(xz)} \cdot \left(\frac{\partial Ex}{\partial - Z - Z_{45}}\right)^2 u^2_{-Z-Z_{45}} + \\ & + \left(\frac{\partial Ex}{\partial Roll(y)}\right)^2 u^2_{Roll(y)} \cdot \left(\frac{\partial Ex}{\partial(Z_{12} - Z - Z_{45})}\right)^2 u^2_{(Z_{12}-Z-Z_{45})} \end{aligned} \tag{6}$$

$$\begin{aligned} u^2 Ey = {} & \left(\frac{\partial Ey}{\partial Pos(y)}\right)^2 u^2_{Pos(y)} + \left(\frac{\partial Ey}{\partial Rx(y)}\right)^2 u^2_{Rx(y)} + \\ & + \left(\frac{\partial Ey}{\partial Rz(y)}\right)^2 u^2_{Rz(y)} + \left(\frac{\partial Ey}{\partial Ort(xy)}\right)^2 u^2_{Ort(xy)} + \left(\frac{\partial Ey}{\partial X_{23}}\right)^2 u^2_{X_{23}} + \\ & + \left(\frac{\partial Ey}{\partial X}\right)^2 u^2_X + \left(\frac{\partial Ey}{\partial Yaw(y)}\right)^2 u^2_{Yaw(y)} \cdot \left(\frac{\partial Ey}{\partial(X_{23} + X)}\right)^2 u^2_{(X_{23}+X)} - \\ & - \left(\frac{\partial Ey}{\partial Pitch(y)}\right)^2 u^2_{Pitch(y)} \cdot \left(\frac{\partial Ey}{\partial(Z_{12} - Z - Z_{45})}\right)^2 u^2_{(Z_{12}-Z-Z_{45})} - \\ & - \left(\frac{\partial Ey}{\partial Ort(yz)}\right)^2 u^2_{Ort(yz)} \cdot \left(\frac{\partial Ey}{\partial(-Z - Z_{45})}\right)^2 u^2_{(-Z-Z_{45})} - \\ & - \left(\frac{\partial Ey}{\partial Roll(x)}\right)^2 u^2_{Roll(x)} \cdot \left(\frac{\partial Ey}{\partial(-Z - Z_{45})}\right)^2 u^2_{(-Z-Z_{45})} - \\ & - \left(\frac{\partial Ey}{\partial Pitch(z)}\right)^2 u^2_{Pitch(z)} \cdot \left(\frac{\partial Ey}{\partial(-Z - Z_{45})}\right)^2 u^2_{(-Z-Z_{45})} \end{aligned} \tag{7}$$

$$u^2Ez = \left(\frac{\partial Ez}{\partial Pos(z)}\right)^2 u^2_{Pos(z)} + \left(\frac{\partial Ez}{\partial Rx(z)}\right)^2 u^2_{Rx(z)} + \\ + \left(\frac{\partial Ez}{\partial Ry(z)}\right)^2 u^2_{Ry(z)} - \left(\frac{\partial Ez}{\partial Roll(y)}\right)^2 u^2_{Roll(y)} \\ \cdot \left(\frac{\partial Ez}{\partial(X_{23}+X)}\right)^2 u^2_{(X_{23}+X)} - \left(\frac{\partial Ez}{\partial Roll(x)}\right)^2 u^2_{Roll(x)} \cdot \\ - \left(\frac{\partial Ez}{\partial Y_{34}}\right)^2 u^2_{Y_{34}} - \left(\frac{\partial Ez}{\partial Pitch(x)}\right)^2 u^2_{Pitch(x)} \cdot \left(\frac{\partial Ez}{\partial Y_{34}}\right)^2 u^2_{Y_{34}} \quad (8)$$

Each geometric error was measured individually and a mathematical model was developed for each one of them, in order to subsequently apply the law of propagation of uncertainties. A detailed description of the model can be observed in [5].

2.1.1. Measurement uncertainty of individual errors

Equation (9) allows estimating the uncertainty associated to the measured orthogonal errors using the mechanical square standard and a LVDT type transducer.

$$D = L_{LVDT} + C_{Sq} + R_{LVDT} + L \cdot \alpha_{Sq} \cdot \Delta T_E \quad (9)$$

where: D is the measured displacement; L_{LVDT} is the reading taken by LVDT; C_{Sq} is the correction due to error of the mechanical square; R_{LVDT} is the resolution of the LVDT; α_{Sq} is the coefficient of thermal expansion of the mechanical square (granite) and ΔT_E is the difference between the mechanical square temperature and the reference temperature.

Equation (10) allows determining the uncertainty associated to the measurement of positioning errors.

$$E_{Pos} = M + R_{CMM} + R_L + \alpha_L L \Delta T_L + \alpha_E L \Delta T_E \quad (10)$$

where: E_{Pos} is the positioning error; M is the value indicated by machine; R_{CMM} is the resolution of the machine; R_L is the resolution of the laser; ΔT_L is the difference between the room temperature and the reference temperature; ΔT_E is the difference between the scale temperature and the reference temperature; α_E and α_L are the coefficients of thermal expansion of the scale (glass) and the laser beam, respectively.

Still, the laser interferometer system has the principle of measurement based on the wavelength of the light. So, room temperature variations cause changes in the wavelength of the light and thus, errors in the measurements are inserted. The calculation of the laser correction coefficient must be done for that the uncertainty can be estimated. Eq. (11) sets a relation between wavelength, frequency and velocity of light.

$$\lambda = \frac{v}{f} \quad (11)$$

where: λ is the wavelength, υ is the velocity of light and f is the frequency.

The velocity of light is constant in vacuum but, through the air, it varies as a function of air temperature, pressure and humidity. Since laser frequency is constant, the wavelength will change with the variation of the velocity of light. The distance D shown in the measurement display of the laser unity corresponds to the number of wavelengths, N, multiplied by a compensation factor, C, and the wavelength in the air, λ_A, as follows:

$$D = N \cdot C \cdot \lambda_A \quad (12)$$

The compensation factor C can be calculated by means of the equation below. N is the wavelength of movement and can be calculated using Eq. (13), where H is the humidity and P is the pressure.

$$C = \frac{10^{12}}{N + 10^{-6}} - 999000 \quad (13)$$

$$N = 0.3836391 \cdot P \cdot \left[\frac{1 + 10^{-6} \cdot P(0.817 - 0.0133 \cdot T)}{1 + 0.003661 \cdot T}\right] - \\ - 3.033 \cdot 10^{-3} H\left(e^{0.057626T}\right) \quad (14)$$

The mathematical model that represents the straightness errors, as well as, pitch and yaw angular errors**,** of all the axes, is given by Eq. (15).

$$E = e + R_L + C_L + Thermaleffect \quad (15)$$

where: E is the error; e is the indicated value by laser; R_L is the resolution of the laser; C_L is the is the coefficient of thermal expansion of the laser beam; ΔT is the variation of the room temperature regarding the reference.

The mathematical model of the roll angular error measurement is given by Eq. (16), where: e is the error; e is the indicated value by the electronic level; R_{Nb} is the resolution of the bubble level; R_{Ne} is the resolution of the electronic level and ΔT is the variation of the room temperature regarding the reference.

$$E = e + R_{Nb} + R_{Ne} + Thermaleffect \quad (16)$$

The mathematical model of the fixed offsets measurement is:

$$L = l + R_{RM} + l \cdot \alpha_{RM} \cdot \Delta T \quad (17)$$

where: l is the measured length; α_{RM} is the coefficient of thermal expansion of mechanical rule; R_{RM} is the resolution mechanical rule and ΔT is the room temperature variation.

2.2. Second model

The calculations are complex and require the calibration of CMM to determine the values of 21 individual geometric errors and measurement of Abbé offsets. Therefore, the complexity of this methodology makes it difficult to be adopted by the majority of the community dedicated to the use CMM.

The present paper proposes alternative mathematical models that are easy to understand and simple to be implemented, in order to popularize the uncertainty calculation of uncertainty measurement in CMM.

2.2.1. Calibration of second CMM

The CMM, type moving bridge, manufactured by Mitutoyo (Fig. 2) was calibrated using a step gauge artifact. The artifact was measured 5 times in 7 different positions in the work volume. The first three positions were parallel to the X, Y, and Z axes, respectively, while the rest were in volumetric diagonals.

This CMM has a resolution of 0.001 mm and a work volume of 300 mm (Axis X) x 400 mm (Axis Y) x 300 mm (Axis Z).

The measurements were carried out at a controlled room temperature of (20 ± 1) °C. A thermo-hygrometer with a digital increment of 0.1 °C and measurement range of (-20 to 60) ºC was used to monitor the temperature. The temperature during calibration was (20.3 ± 0.2)° C.

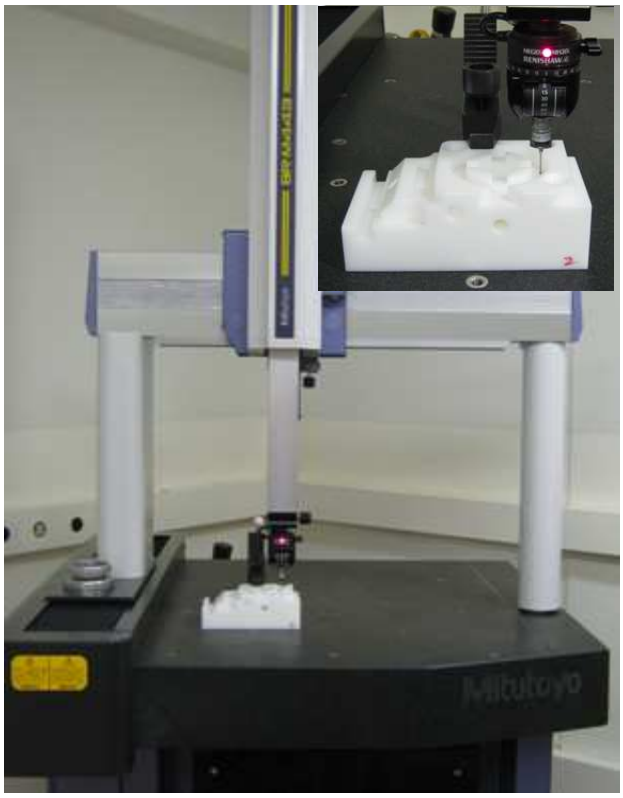

Figure 2. Coordinate Measurement Machine (CMM) used in the second methodology.

2.2.2. New formulation

This new formulation is presented in Eqs. (18, 19 and 20).

$$u(X_{machine}) = u(X) = \Delta R_{CMM} + \Delta IC_{CMM}(X_i) + \Delta EA + \\ + X\alpha\Delta T + X\alpha\delta T \quad (18)$$

$$u(Y_{Machine}) = u(Y) = \Delta R_{CMM} + \Delta IC_{CMM}(Y_i) + \Delta EA + \\ + Y\alpha\Delta T + Y\alpha\delta T \quad (19)$$

$$u(Zmachine) = (u(Z) = \Delta R_{CMM} + \Delta IC_{CMM}(Z_i) + \Delta EA + \\ + Z\alpha\Delta T + Z\alpha\delta T \quad (20)$$

The uncertainty of each volumetric component is as function of: corrections associated to the CMM resolution (ΔR); errors of the CMM probing system (ΔEA); uncertainty associated with the CMM indication system (ΔIC_{CMM}); corrections due to the distancing of the temperature in relation to 20°C (ΔT_{20}) and corrections due to temperature variation during measurement ($\Delta\delta T$).

To calculate uncertainty of any geometry must still consider the variability associated with the results obtained for different measuring cycles. As an example, are shown the equations for determination of uncertainty of measurement of circularity and cylindricity, Eqs (21) and (22).

$$D_{CIR} = \Delta s(D_{CIR}) + \Delta P\,max + \Delta P\,min \quad (21)$$

$$D_{CYL} = \Delta s(D_{CYL}) + \Delta P\,max + \Delta P\,min \quad (22)$$

These equations take into account the variability of the circularity deviations ($\Delta s(D_{CIR})$) or cylindricity deviations ($\Delta s(D_{CYL})$), considering the *n* measurement cycles and the corrections associated with the furthest point in relation to the centre (*Pmax*) and the point least distant from the centre (*Pmin*).

On the other hand, the uncertainty of those two points is obtained by Eq. (23).

$$\Delta P\,max = \Delta P\,min = \Delta R + \Delta EA + \Delta IC_{CMM} + \\ + L\Delta\alpha\Delta T_{20} + L\Delta\alpha\delta T \quad (24)$$

L is given by Eq. (25). Where X_i, Y_i and Z_i are the coordinates of the point *Pmax* and *Pmin*, respectively.

$$L = \sqrt{X_i^2 + Y_i^2 + Z_i^2} \quad (25)$$

Substituting (25) in (21) and (22) and applying the law of propagation of uncertainty, Eqs. (26) and (27) are obtained.

$$u_C^2(D_{CIR}) = \left(\frac{\partial D_{CIR}}{\partial \Delta s(Dcir)}\right)^2 \cdot [u(\Delta s(Dcir))]^2 + \\ +2\cdot\left[\left(\frac{\partial D_{CIR}}{\partial \Delta R}\right)^2 \cdot [u(\Delta R)]^2\right] + 2\cdot\left[\left(\frac{\partial D_{CIR}}{\partial \Delta EA}\right)^2 \cdot [u(\Delta EA)]^2\right] + \\ +2\cdot\left[\left(\frac{\partial D_{CIR}}{\partial \Delta I}\right)^2 \cdot [u(\Delta I)]^2\right] + 2\cdot\left[\left(\frac{\partial D_{CIR}}{\partial \Delta T_{20}}\right)^2 \cdot [u(\Delta T_{20})]^2\right] + \\ +2\cdot\left[\left(\frac{\partial D_{CIR}}{\partial \Delta \delta T}\right)^2 \cdot [u(\Delta \delta T)]^2\right] \quad (26)$$

$$u_C^2(D_{CYL}) = \left(\frac{\partial D_{CYL}}{\partial \Delta s(D_{CYL})}\right)^2 \cdot [u(\Delta s(D_{CYL}))]^2 + \\ +2\cdot\left[\left(\frac{\partial D_{CYL}}{\partial \Delta R}\right)^2 \cdot [u(\Delta R)]^2\right] + 2\cdot\left[\left(\frac{\partial D_{CYL}}{\partial \Delta EA}\right)^2 \cdot [u(\Delta EA)]^2\right] + \\ +2\cdot\left[\left(\frac{\partial D_{CYL}}{\partial \Delta I}\right)^2 \cdot [u(\Delta I)]^2\right] + 2\cdot\left[\left(\frac{\partial D_{CYL}}{\partial \Delta T_{20}}\right)^2 \cdot [u(\Delta T_{20})]^2\right] + \\ +2\cdot\left[\left(\frac{\partial D_{CYL}}{\partial \Delta \delta T}\right)^2 \cdot [u(\Delta \delta T)]^2\right] \quad (27)$$

The standard uncertainty related to $s(D_{CIR})$ and $s(D_{CYL})$ can be calculated as shown in Eq. (28).

$$s(D_{CIR}) = s(D_{CYL}) = \frac{s}{\sqrt{n}} \quad (28)$$

Where s is the standard deviation of the deviation readings and n is the total number of measurement cycles.

The correction due to the CMM resolution is given by Eq. (29).

$$u(\Delta R) = \frac{R}{2\cdot\sqrt{3}} \quad (29)$$

The correction due to errors of the CMM probing system is given by Eq. (30).

$$u(\Delta EA) = \frac{EA}{\sqrt{6}} \quad (30)$$

The correction due to the uncertainty associated with the CMM indication system is given by Eq. (31).

$$u(\Delta I) = \sqrt{\left(\frac{\Delta I_{(x)}}{k_{(x)}}\right)^2 + \left(\frac{\Delta I_{(y)}}{k_{(y)}}\right)^2 + \left(\frac{\Delta I_{(z)}}{k_{(z)}}\right)^2} \quad (31)$$

Both variables related to room temperature variation were measured using the same measurement system. Therefore, they were treated as correlated. The correction due to the distancing of the temperature in relation to 20 °C (ΔT_{20}) is determined using Eq. (32).

$$u(\Delta T_{20}) = \sqrt{\left(\frac{\Delta T}{\sqrt{3}}\right)^2 + \left(\frac{\Delta R_T}{2\cdot\sqrt{3}}\right)^2 + \left(\frac{\Delta I_T}{k_T}\right)^2} \quad (32)$$

where ΔT is the difference between the room temperature and 20 °C; ΔR_T is the correction in relation to the thermometer resolution and ΔI_T is the uncertainty associated with the thermometer indication system.

The uncertainty due to temperature variation during measurement is given by Eq. (33).

$$u(\Delta \delta T) = \sqrt{\left(\frac{Var(T)}{\sqrt{3}}\right)^2 + \left(\frac{\Delta R_T}{2\cdot\sqrt{3}}\right)^2 + \left(\frac{\Delta I_T}{k_T}\right)^2} \quad (33)$$

3. RESULTS AND DISCUSSION

3.1. Results for first methodology

The uncertainties associated to the components of the volumetric error *Ex* were calculated (Fig. 3). It was observed that uncertainty values varied from 2,79 to 2,86 µm and presented similar behavior at the different evaluated planes. The greatest influences upon the total uncertainty of the volumetric error *Ex* component were the orthogonality errors between axes *X*-*Y* and *X*-*Z* and *Y*-axis roll error. This fact is assured by the combination of error values and their uncertainties with values and uncertainties of fixed offsets, which are, in this case, Y_{34}, Z_{45} e Y_{12}, respectively.

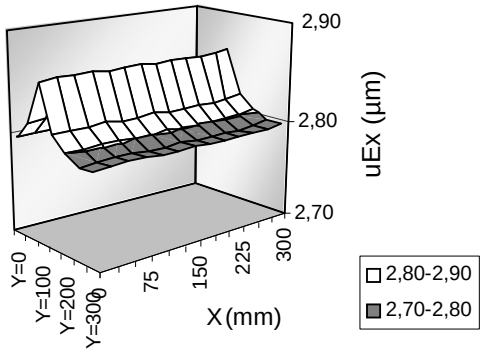

Figure 3 - Uncertainty measurement of *Ex*, to Z=150 mm (First methodology)

The uncertainty associated to the volumetric error component *Ey* presents nearly constant values, which vary between 4.00 and 4.03 µm (Fig. 4). Component *Ey* presented the largest uncertainty values at reference temperature. This fact may be attributed to several factors: the sinthesization equation of that component presenting a high number of influence variables; the orthogonality error magnitude between axes *Y* and *Z* and fixed arm Z_{12}, as well as the uncertainty associated to them.

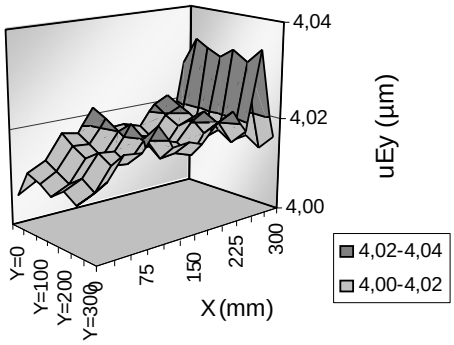

Figure 4 - Uncertainty measurement of *Ey*, to *Z*=150 mm (first methodology)

The uncertainty associated to the volumetric error component *Ez* presents small and nearly constant values, which vary between 1.98 and 2.00 µm (Fig. 5).

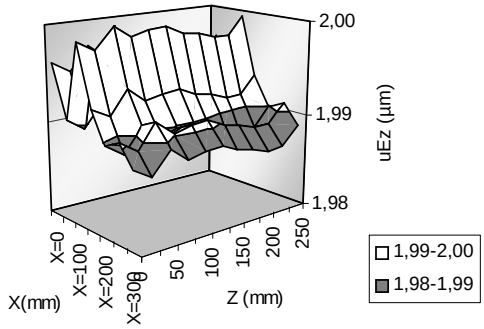

Figure 5. Uncertainty measurement of *Ez*, to *Y*=150 mm (first methodology)

Such values are smaller than the calculated uncertainty for *Ex* and *Ey* because of the reduced number of influence variables in the synthesization equation of *Ez*. Moreover, there are orthogonallity errors in the referred equation. The fractions that presented the greatest influence over total uncertainty of component *Ez* were angular errors *Roll(X)* and *Roll(Y)*. Mean and standard deviation values of *Ez* uncertainty are similar at different planes.

3.2. Results for second methodology

The following, uncertainties associated to the components of the volumetric error ware estimated considering the new formulation. The results are shown below.

Figure 6 shows the values for volumetric error Ex. It was observed that uncertainty values varied from 1.97 to 2.25 and presented a linear behavior and increasing to the values of that X and Y increases.

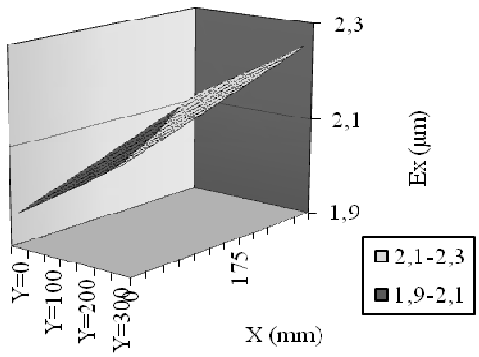

Figure 6 - Uncertainty measurement of *Ex*, to Z=150 mm (second methodology)

The uncertainty associated to the volumetric error component Ey (Fig. 7) varies between 1.97 and 2.26 µm and, too, presents a linear behavior and increasing to the values of X and Y increases.

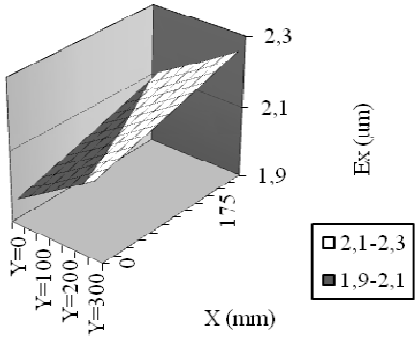

Figure 7 - Uncertainty measurement of *Ey*, to *Z*=150 mm (second methodology)

The uncertainty associated to the volumetric error component *Ez* (Fig. 8) presents values, which vary between 1.98 and 2.21 µm.

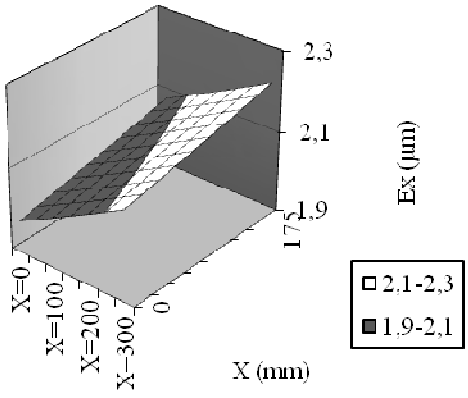

Figure 8. Uncertainty measurement of *Ez*, to *Y*=150 mm (second methodology)

3.3. Examples of application of the second methodology

The mean values of the diameters measured in the experiments are shown in Table 1.

Table 1. Diameters of the features measured in the tests.

Measurand	Diameter (mm)	
	Mean	Standard deviation
1	8.008	0.004
2	19.936	0.016
3	47.953	0.013
4	67.957	0.005

Table 2 shows circularity and cylindricity values for all the features measured in the tests.

Table 2. Circularity and cylindricity measurements.

Measurand	Circularity deviation (µm)		Cylindricity deviation (µm)	
	Mean	Standard deviation	Mean	Standard deviation
1	10	2	11	2
2	57	4	61	5
3	95	5	102	5
4	92	5	105	3

The values for the combined standard uncertainty (u_c) and for the expanded standard uncertainty (*Up*) associated with the measurements of the circularity and cylindricity for the four measurands are shown in Fig. 9 and 10. These values were obtained using the new formulation proposed in this paper.

It should be pointed out that two significant digits were added during the calculations to minimize rounding errors.

Circularity deviation uncertainty

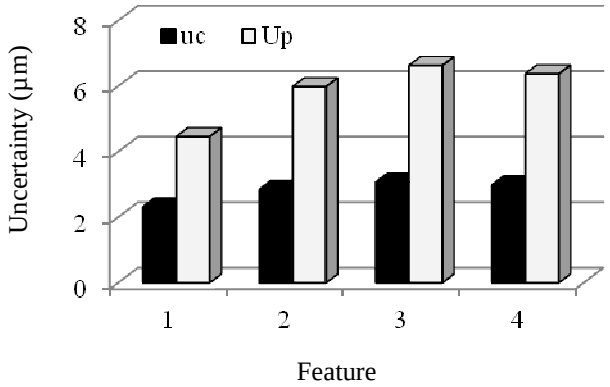

Figure 9. Combined and expanded standard uncertainties for the circularity deviation measurements.

According to Figure 9, the combined uncertainty for the circularity deviation measurements varied between 2.3 and 3.1 µm. The values for the expanded uncertainty varied between 4.5 and 6.3 µm, for a coverage factor of 95.45 %.

Cylindricity deviation uncertainty

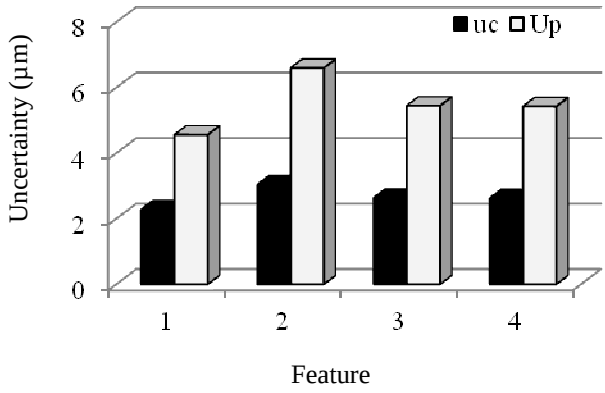

Figure 10. Combined and expanded standard uncertainties for the cylindricity deviation

Figure 10 shows that the combined uncertainty for the cylindricity deviation measurements varied between 2.3 and 3.0 µm. The values for the expanded uncertainty varied between 4.6 and 6.6 µm, for a coverage factor of 95.45 %.

In all cases, the largest contribution for the final uncertainty was given by the CMM probing error and by the variability of the values of circularity and cylindricity deviations for each measurand.

The simplified models here proposed, implemented using an Excel spreadsheet, proved to be viable and easy to apply to evaluate the uncertainty measurements associated to both geometric deviations here investigated.

4. CONCLUSIONS

In the end of this work, the following conclusions may be presented.

The procedures described in [1] have been efficient to determine the uncertainty associated the components of the volumetric error at any point of the work volume of the evaluated machine at given conditions. By determining the effects of variables in three-dimensional uncertainty information was obtained.

For the first methodology, the uncertainties associated to the components of the volumetric error (*Ex*, *Ey* e *Ez*) were homogeneously perceived at several planes. It values close to 1,4, 1,3 and 1,2 µm, for X, Y and Z axis, respectively.

For the second methodology, the uncertainties associated to the components of the volumetric error (*Ex*, *Ey* e *Ez*) were homogeneously perceived at several planes. It values close to 2.25, 2.26 and 2.21 µm, respectively.

The uncertainty values obtained for the first methodology are higher because the number of input variables is greater, too.

The second methodology proposed in this paper have proved to be viable and of easy application to evaluate volumetric error component uncertainty measurement.

The observed differences in uncertainty values obtained by both methodologies can be justified because they were

used two different machines. Still, each machine was calibrated using a different calibration procedure.

5. ACKNOWLEDGEMENT

The authors are grateful to FAPEMG by the financial support in this work.

6. REFERENCES

[1] ISO TAG 4/WG 3. Guide to the Expression of Uncertainty in measurement (GUM), Geneva: International Organization for Standardization. 2008.

[2] A. M. Balsamo. Di Ciommo, R. Mugno, B.I. Rebaglia, E. Ricci, R. Grella "Evaluation of CMM uncertainty through Monte Carlo simulations". Annals of the CIPR 48(1). Pp. 425-8. 1999.

[3] Bosch JA. Coordinate measuring machines and system. New York: Marcel Dekker; 1995. p. 444.

[4] R.A. Valdés, Modelo de Sintetização de Erros Termicamente Induzidos em Máquinas de Medir a Três Coordenadas. Tese (Doutorado) – EESC-USP, São Carlos, Brasil. p.190. 2003.

[5] ISO/TR 16015: "Geometrical product specifications (GPS) – Systematic errors and contributions to measurement uncertainty of length measurement due to thermal influences". Technical report. 2003.

[6] C.C. Souza, Valdés. R.A. Costa, H.L. Piratelli-Filho, A. A contribution to the measurement of circularity and cylindricity deviations. 21st Brazilian Congress of Mechanical Engineering. Natal, RN, Brazil, 2011, 10p.